

PCCP

Physical Chemistry Chemical Physics

Accepted Manuscript

This article can be cited before page numbers have been issued, to do this please use: R. Mondal and M. G. Basavaraj, *Phys. Chem. Chem. Phys.*, 2019, DOI: 10.1039/C9CP03008E.



This is an Accepted Manuscript, which has been through the Royal Society of Chemistry peer review process and has been accepted for publication.

Accepted Manuscripts are published online shortly after acceptance, before technical editing, formatting and proof reading. Using this free service, authors can make their results available to the community, in citable form, before we publish the edited article. We will replace this Accepted Manuscript with the edited and formatted Advance Article as soon as it is available.

You can find more information about Accepted Manuscripts in the [Information for Authors](#).

Please note that technical editing may introduce minor changes to the text and/or graphics, which may alter content. The journal's standard [Terms & Conditions](#) and the [Ethical guidelines](#) still apply. In no event shall the Royal Society of Chemistry be held responsible for any errors or omissions in this Accepted Manuscript or any consequences arising from the use of any information it contains.

Cite this: DOI: 00.0000/xxxxxxxxxx

Influence of drying configuration on patterning of ellipsoids - concentric rings and concentric cracks[†]

Ranajit Mondal and Madivala G. Basavaraj*

Received Date
Accepted Date

DOI: 00.0000/xxxxxxxxxx

Evaporation of colloidal dispersion leading to the patterning of particles, is a simple and elegant route for controlling the self-assembly of particles on solid surface. In this article, we demonstrate that the configuration in which the colloidal dispersion is dried greatly influences the patterning of particles on solid surface after complete evaporation of the solvent. The evaporation experiments are carried out using well-characterized stable aqueous dispersion of hematite ellipsoids and polystyrene spheres. The drying of particle laden sessile drops always give “*coffee – ring*” deposit irrespective of particle concentration. At particle concentration ≥ 0.3 wt% circular cracks appear in the annular region of the coffee-ring deposit owing to the ordered arrangement of ellipsoids. In stark contrast, the deposits formed by drying dispersion of ellipsoids in the sphere-on-plate configuration shows a transition from “*concentric – ring*” to “*concentric – crack*” in the micro-structure of the particulate film with increase in the concentration of particles. Further, our experimental findings reveal that long-ranged circular cracks and long-ranged assembly of particles can be achieved by drying of dispersion in sphere-on-plate configuration. While the nature of patterns - that is - coffee-rings and concentric rings - are independent of the shape of the particle, strikingly different crack morphology is shown to be dictated by the shape of the particles in the dispersion. The results presented show that the drying of colloidal dispersion in the sphere-on-plate configuration enables the fabrication of long ranged ordered assembly of particle over area as large as few square millimeters.

1 INTRODUCTION

The evaporation of solvent from a drying drop containing insoluble solutes is crucial to materials engineering, medicine, agriculture and is also significant to many technological applications as well^{1–3}. The most studies of drying of dispersion containing particles is studied in the sessile configuration (i.e. drop on substrate)^{4–12}. The drying of a sessile particle-laden drop on a solid substrate leads to a ring-like deposit of particles at the periphery of the drop, widely known as “*coffee – ring*” deposit⁴. Such a deposit is formed due the migration of particles to the pinned contact line (CL) of the drop as a result of the radial outward capillary flow of the carrier fluid^{4,5}. Controlling the morphology of the final particulate deposit on the substrate formed by drying of dispersion containing particles has received considerable attention. This has been exploited to control the self-assembly of particles on solid substrates. The deposit patterns and assemblies of particles realised through this route, in particular, find appli-

cations in the area of paint technology, coatings, catalysis, and in the fabrication of photonic materials¹³.

The dried deposit patterns on the substrate obtained by drying of dispersion containing particles can be tailored by controlling capillary flow⁴, temperature induced Marangoni-Benard convection^{14–16}, wettability of the substrate^{10,17–19}, particle shape and size⁸, particle-particle and particle-substrate DLVO (Derjaguin-Landau-Verwey-Overbeek) interactions^{9,11}. In addition to the aforementioned factors, the configuration in which the particle laden dispersion dries is also an important factor that dictates the final deposit patterns and the self-assembly of particles in the deposit. In this context, the drying of dispersion under confinement provides a great control over the evaporation of solvent and associated internal flows that contribute to the transport and self-assembly of particles. To date, few elegant methods such as drying of dispersion confined between parallel plate²⁰, sphere-on-plate^{21–24}, wedge geometry²⁵, cylindrical confinement i.e., drying in thin capillaries and vertical deposition²⁶ have emerged. These methods provide precise control of the evaporation process that enable the directed self-assembly of the particles such that intriguing deposit patterns can be achieved. The drying of particle laden dispersion on solid surfaces that results in the

Polymer Engineering and Colloid Science Laboratory (PECS Lab), Department of Chemical Engineering, Indian Institute of Technology Madras, Chennai-600036, India.
E-mail: basa@itm.ac.in

[†] Electronic Supplementary Information (ESI) available

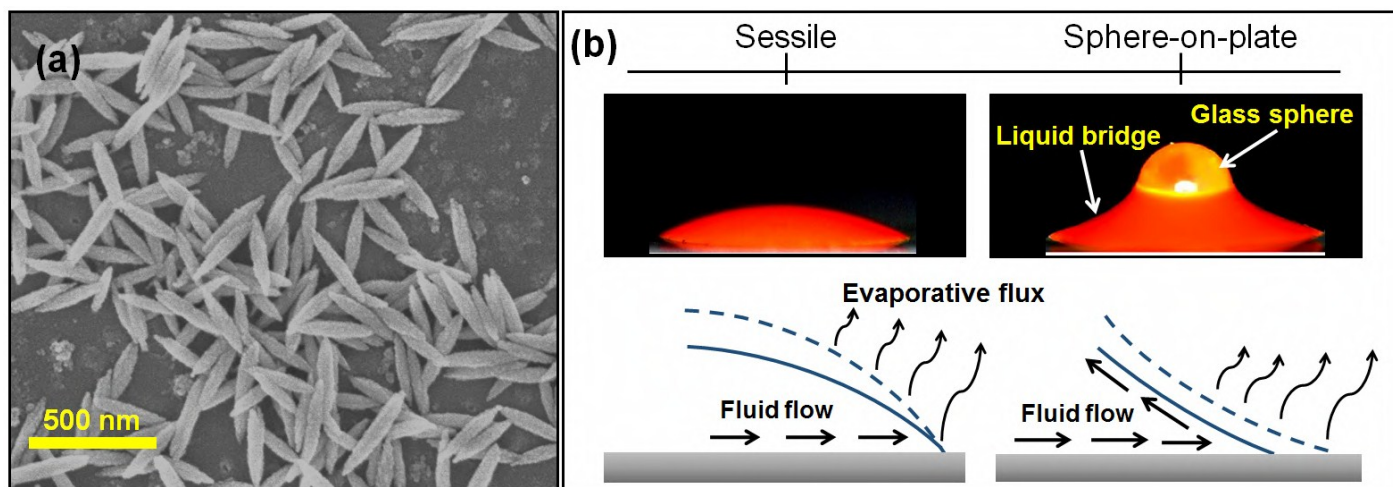


Fig. 1 (a) High resolution scanning electron microscopy (HR-SEM) image of the hematite (α - Fe_2O_3) ellipsoidal particles used in the drying experiments. These particles synthesized by forced hydrolysis method have a mean aspect ratio, $\alpha=5.18 \pm 0.5$. (b) The drying of dispersion of hematite ellipsoids in sessile and sphere-on-plate configurations and the corresponding schematic representing the direction of the fluid flow during the evaporation process.

particulate film often exhibit cracks, similar to those commonly observed in the dried mud²⁷ and old paintings²⁸. Although these cracks are unacceptable in many applications pertaining to coatings. The periodic cracks formed in a controlled manner find potential application as lithography template for fabricating nano and micro-channels (for nano and micro-fluidics) and in optical grafting. The crack in particulate film arise due to the release of excess stress energy which is accumulated during the course of drying^{29,30}. The crack morphology and the ordered assembly of particles can be controlled by tuning various parameters, such as shape of particles³¹, drying condition³², external fields³³ (electric or magnetic fields applied during drying) etc.

We consider well-characterized model colloidal dispersion and report the experimental findings on the influence of drying configuration to the morphology of the final dried deposition patterns and self-assembly of particles. The effect of the concentration of particles and particle shape are studied. To this end, the dispersion of colloidal ellipsoids and spheres are dried in the sessile and sphere-on-plate configuration under identical experimental conditions. The colloidal dispersion consisting of hematite ellipsoids of aspect ratio, $\alpha \sim 5.2$ at various particle concentrations (0.12-4 wt%) are evaporated in the two different drying configurations. The dispersion of charged stabilized hematite ellipsoids when dried in the sessile drop configuration, is known to form coffee-ring like deposit^{9,10}. However, the drying of the dispersion in the sphere-on-plate configuration at the same temperature and relative humidity show a transition from a deposit with “concentric – ring” to a deposit with long ranged “concentric – crack” as the concentration of ellipsoids in the dispersion is increased. The contrasting spatial arrangement of particles in the deposits formed by drying of dispersion in the two drying configurations is attributed to the difference in the drying kinetics. Furthermore, we also reports that the nature of crack depends on the shape of the constituent particle and a long ranged

assembly of particle can be achieved over area as large as few square millimeters by drying of colloidal dispersion in the sphere-on-plate configuration.

2 MATERIALS AND METHODS

2.1 Synthesis of hematite ellipsoids

The hematite (α - Fe_2O_3) ellipsoid particles used in the droplet drying experiments are synthesized using forced hydrolysis of Fe^{+3} in the presence of urea³⁴. The aspect ratio ($\alpha = L/D$) of the ellipsoid, defined as the ratio of length (L) to the diameter (D) of the particle, is tuned by varying the quantity of NaH_2PO_4 added to the reaction mixture. In a typical synthesis process of hematite ellipsoid, 9.24 g of iron (III) perchlorate, $Fe(ClO_4)_3$ (Alfa aesar, India), 1.2 g of urea, $CO(NH_2)_2$ (Merck, India) and 0.15 g sodium di-hydrogen phosphate, NaH_2PO_4 (Merck, India) are added to 200 ml Milli-Q water taken in a piranha (70% H_2SO_4 and 30% H_2O_2 by volume) cleaned Pyrex bottle. Thereafter, with all the reagents the Pyrex bottle is kept in a preheated oven at 100°C for 24 h. After the reaction time the reaction product is cooled overnight, the synthesized particles are separated from the reaction product by centrifugation for ~ 30 min at a fixed 6000 rpm and washed multiple times with de-ionized water until a clear supernatant is obtained. Finally to stabilize the suspension, pH of the hematite ellipsoid suspension is adjusted to 2 by adding aqueous HNO_3 to the solution. Under these conditions, the particles are highly charged with a zeta potential of +40 mV (measured in 0.0001 M NaCl) i.e., the dispersion are charge stabilized and do not show any gravity settling. High resolution scanning electron microscope (HR-SEM) characterization reveals that the synthesized hematite ellipsoids are highly mono-disperse as shown in Fig.1 (a) with $\alpha = 5.18 \pm 0.5$ ($L = 317 \pm 34$ nm and $D = 61 \pm 7$ nm).

2.2 Evaporation of droplet

The evaporation experiments are performed by placing a drop of colloidal dispersion with various particle concentrations (ϕ

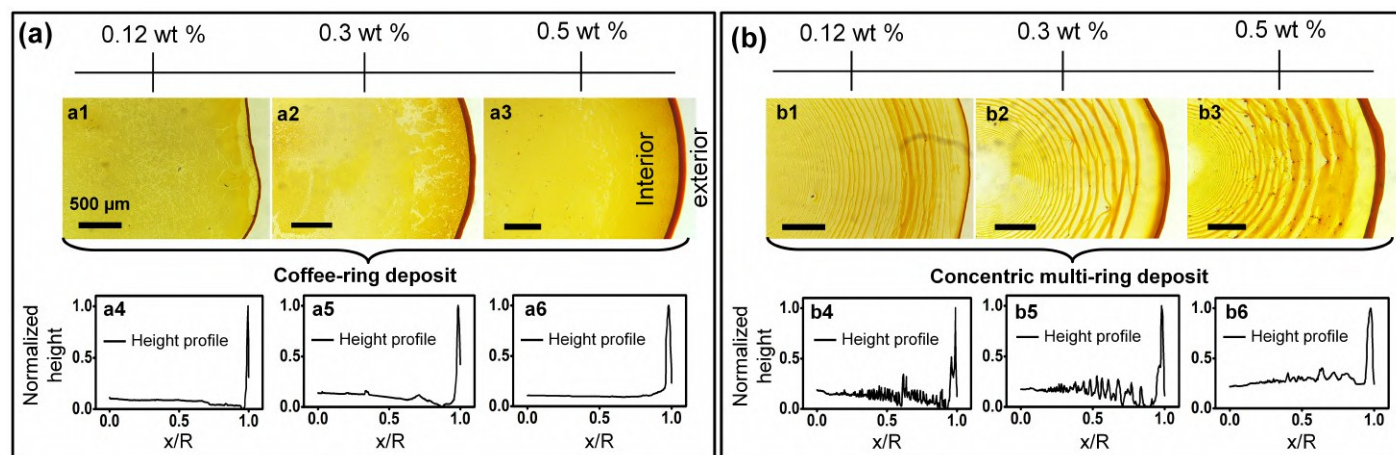


Fig. 2 Evaporation of dispersions containing hematite ellipsoids with particle concentration ranging from 0.12 wt% to 0.5 wt%. As evident, drying configuration dictates the patterning of particles on the substrate. The microscopy images show the part of the final particulate deposit obtained upon complete evaporation of the solvent. **(a)** Drops dried in sessile mode always show coffee-ring at the three phase contact line (top panel, a1-a3), further confirmed by the height profiles (bottom panel, a4-a6). **(b)** Dried deposit obtained from the sphere-on-plate configuration show deposit with concentric-rings (top panel, b1-b3) and the corresponding height profiles show multiple spikes associated with the concentric-rings in the patterns (bottom panel, b4-b6). The scale bar in each image corresponds to 500 μm .

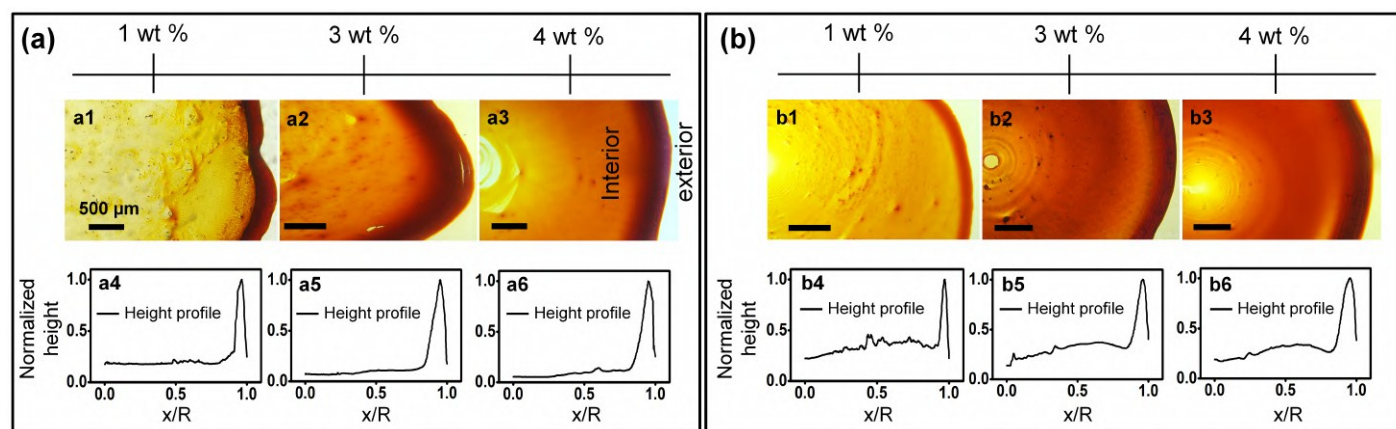


Fig. 3 Evaporative patterns by drying of dispersions containing hematite ellipsoids with particle concentration ranging from 1 wt% to 4 wt%. **(a)** Similar to the deposit obtained at lower particle concentration, the sessile drops always leave a coffee-ring (top panel, a1-a3). The height and width of the ring increases with increase in the concentration of particles as evident from height profiles (bottom panel, a4-a6). **(b)** The microscopy images of the particulate film obtained by the drying of dispersion in the sphere-on-plate configuration shows the disappearance of the concentric-ring deposit (top panel, b1-b3). The height profiles confirm significant accumulation of particles in the interior of the deposit compared to those formed by sessile drying mode (bottom panel, b4-b6). The scale bar in each image corresponds to 500 μm .

$\approx 0.12 - 4 \text{ wt}\%$) of known volume ($\sim 5 \mu\text{l}$) in the sessile and sphere-on-plate configurations as shown in Fig.1 (b). The glass slides are used as substrate for the drying experiments. Prior to the experiment, the glass substrates are soap cleaned followed by cleaning with acetone and then dried using N_2 gas. The contact angle (θ_0) of water drop placed on the substrate found to be $25 \pm 5^\circ$ indicates its hydrophilic nature. For the drying of dispersion in the sphere-on-plate configuration, an acid washed glass sphere (Sigma-Aldrich) of diameter $\sim 1 \text{ mm}$ is first fixed to a syringe tip with the help of commercially available adhesive (Fevicol). The clean glass substrate placed on a movable stage is brought in contact with the glass bead to create the sphere-on-plate geometry. The colloidal dispersion is placed around the sphere giving rise to the initial configuration of the dispersion

drying in sphere-on-plate mode, as shown in Fig.1 (b). All the drying experiments in this studies are carried out at a constant temperature of $25 \pm 3^\circ \text{C}$ and relative humidity (RH) of $45 \pm 5\%$. To compare the effect of particle shape in the final dried particulate deposit similar experiments are performed at various particle concentrations ($\phi \approx 0.12 - 4 \text{ wt}\%$) using the suspension of charge stabilized poly-styrene (PS amidine latex) (Thermo fisher scientific) of particle diameter, $d = 200 \pm 20 \text{ nm}$. The experiments are performed under identical drying conditions and with the same droplet volume in the sessile and sphere-on-plate configurations.

2.3 Imaging and analysis of the deposit patterns

The drying of colloidal dispersion leads to the formation of a deposit of particulate film. The images of the final dried particu-

late deposits are captured by Dino-Lite digital microscope (AnMo Electronics Corporation, Taiwan) and also analyzed using optical microscopy (Leica, Germany). The thickness of the film of particulate deposits are confirmed by an optical surface-profiler (Bruker, Contour GT-1, Germany). To study the drying kinetics Goniometer (Kruss, Germany) is used and finally high resolution scanning electron microscopy (HR-SEM) facility is used to unravel the self-assembly of the particles in the final dried particulate film.

3 RESULTS AND DISCUSSION

3.1 Drying configuration influences the final deposit patterns

The part of the final particulate deposit patterns left on the substrate after the drying of dispersion containing colloidal ellipsoids at various particle concentrations ($\phi \approx 0.12 - 4 \text{ wt}\%$) in the two different configurations (i.e. sessile and sphere-on-plate) are shown in Fig.2 and Fig.3. The full length view of the dried deposits are shown in Fig. S1 in the ESI†. As shown in Fig.2 (a) and Fig.3 (a), the drops that are dried in the sessile configuration always leaves a “coffee-ring” deposit i.e., most of the particles are deposited at the three phase contact line of the drying drop. Such ring-like deposits form as a result of an outward capillary flow that transports the particles from the interior of the drop to the contact line⁴, as schematically shown in Fig.1 (b). This capillary flow originates due to the pinning of the droplet and the non-uniform evaporative flux along the drop surface⁵. The ring-like deposits are observed irrespective of the particle concentration. However, with increase in the concentration of particles in the drying sessile drops, the height and width of the ring increase. These particulate deposits are further characterized by plotting the radial variation in the height measured by an optical surface profilometer as depicted in Fig.2 (a) and Fig.3 (a).

In marked contrast to the evaporation of drops in the sessile mode, the dispersions dried in the sphere-on-plate configuration under identical conditions leave deposit with multiple “concentric – ring” which is more prominent at lower concentration of particle in the dispersion ($\phi \approx 0.12-0.5\%$) as shown in Fig.2 (b). The formation of concentric-ring deposit is further confirmed from the height profile measurements shown in Fig.2 (b). As evident in the figure, the normalized height vs. x/R (where x and R respectively, are the distance from the center of the deposit and the radius of the deposit) shows multiple peaks corresponding to the formation of concentric-rings in the interior region of the dried deposits. The number of concentric-rings as shown in Fig.2 (b) reduce as the concentration of particles in the dispersion increases from $\phi \approx 0.12 \text{ wt}\%$ to $\phi \approx 0.50 \text{ wt}\%$. However, the concentric-rings in the dried deposit completely disappear when the dispersions at $\phi \geq 1 \text{ wt}\%$ are evaporated as evident in Fig.3 (b). The microscopy images and the corresponding height profile measurements shown in Fig.3 (a) and in Fig.3 (b) reveal the presence of significant quantity of particles accumulated in the interior of the deposit when dispersions are dried in the sphere-on-plate configuration as against the sessile mode. The height profiles of the particulate deposits clearly show that a large num-

ber of particles are accumulated at the edge of the deposit (note that the width as well as height is significantly large). This is due to the pinning of the contact line during the early period of drying, which subsequently de-pins at a later stage which will be discussed further in the next section. To confirm the influence of droplet volume, identical experiments are carried with dispersions of $\sim 2 \mu\text{l}$ volume and the final deposit patterns are found to be qualitatively similar to that obtained by drying $\sim 5 \mu\text{l}$ volume dispersions as shown in the Fig. S3 in the ESI†. Moreover in this study the dispersions that are dried are deposited on solid surfaces such that the drops are nearly axi-symmetric within the experimental uncertainties. To understand the effect of drying configuration on the strikingly different patterning of the particles on solid surfaces, it is crucial to study and compare the drying kinetics of the evaporating particle laden dispersion in the sessile and sphere-on-plate configuration.

3.2 Evaporation kinetics: sessile vs. sphere-on-plate

As soon as aqueous dispersion is placed on the solid substrate, the temporal evolution of diameter of the three phase contact line (aqueous phase-air-flat substrate) in the two drying configurations is monitored. As shown in Fig.4 (a) ($\phi \sim 0.5 \text{ wt}\%$) and Fig.4 (b) ($\phi \sim 3 \text{ wt}\%$), the drops dried in the sessile configuration, evaporate in the constant contact radius (CCR) mode wherein, the drop contact radius remains constant and the height of the drop decrease monotonically for majority of the drying time. A similar observation is reported in the literature when a sessile drop is dried on a hydrophilic substrate ($\theta_0 < 90^\circ$)^{10,35}. It is observed that the sessile drops dry in the CCR mode for a duration of $\sim 0.65t_f$ to $0.75t_f$, where t_f is the total evaporation time, thereafter the drop continuously starts to de-pin. It is worth mentioning that the drops dried on a hydrophilic substrate ($\theta_0 < 90^\circ$) starts to de-pin when $\theta(t) < \theta_R$ where, $\theta(t)$ is the instantaneous contact angle, and θ_R is the receding contact angle^{36,37}. The aqueous dispersion placed on an “ideal” i.e., physically and chemically homogeneous smooth solid substrate, assumes an equilibrium state characterized by initial radius R_0 and equilibrium contact angle θ_0 which satisfies the Young-Laplace equation,

$$\gamma \cos \theta_0 + \gamma_{SL} - \gamma_{SV} = 0 \quad (1)$$

where γ , γ_{SL} , and γ_{SV} are the interfacial tensions of the liquid-vapour, solid-liquid, and solid-vapour interfaces, respectively. However, most substrates including those used in our experiments possess nano-scale heterogeneities that help in pinning of the liquid leading to the formation of a contact line (CL). In such cases, a pinning force per unit length acts at the contact line while the dispersion deposited on the solid substrate approaches a quasi-equilibrium state³⁸. During drying of dispersion, the contact diameter as well as the contact angle continuously evolve with time and so would be the pinning force. Therefore, the force balance at the three phase contact line takes the following form³⁸,

$$F_p(t) = \gamma \cos \theta(t) + \gamma_{SL} - \gamma_{SV} \quad (2)$$

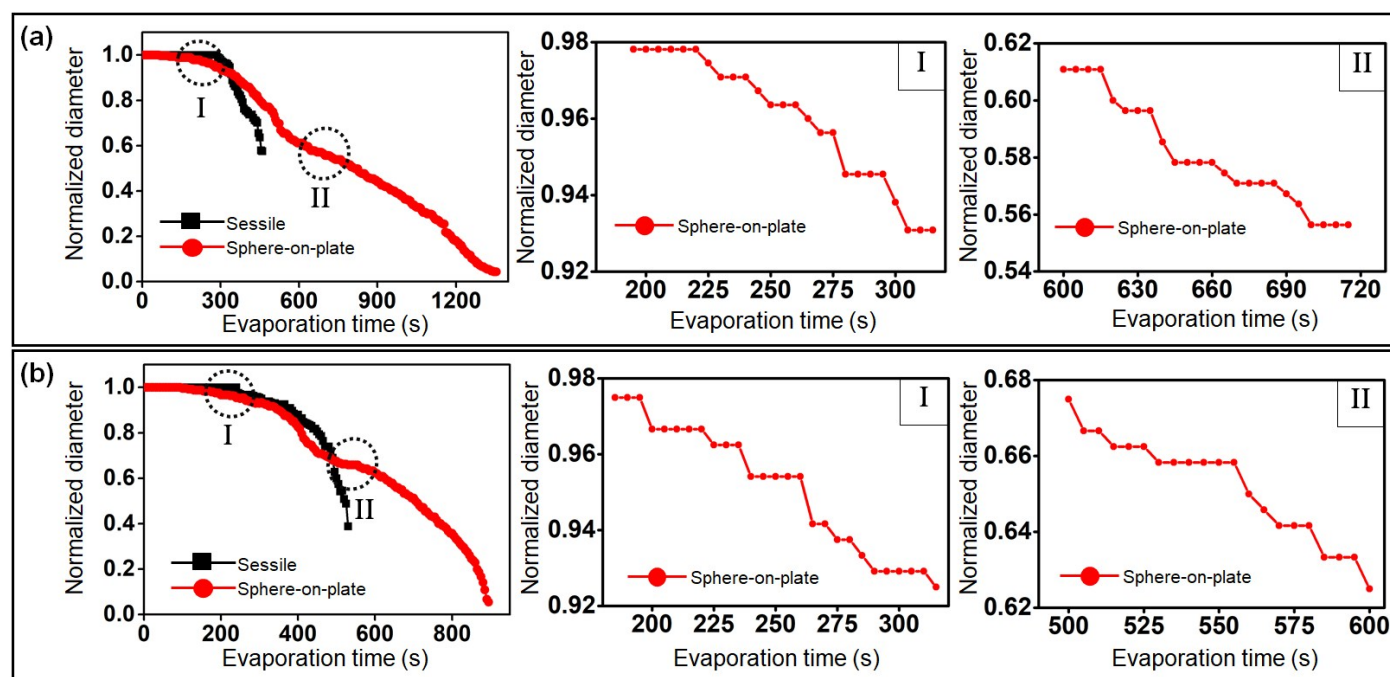


Fig. 4 Evaporation kinetics - drying of dispersion containing ellipsoids of particle concentration (a) $\phi \sim 0.5\text{wt}\%$ and (b) $\phi \sim 3\text{wt}\%$ in sessile and sphere-on-plate configuration. The temporal variation of the diameter of the contact line (normalized by the initial diameter of the contact line) with evaporation time confirms that for majority of drop life time, the sessile drop dries in constant contact radius (CCR) mode. However, an early de-pinning is observed in the case of dispersions dried in the sphere-on-plate configuration. Drying dispersions in this mode exhibit characteristic *stick-slip* motion evident from the plots corresponding to the encircled region I and II.

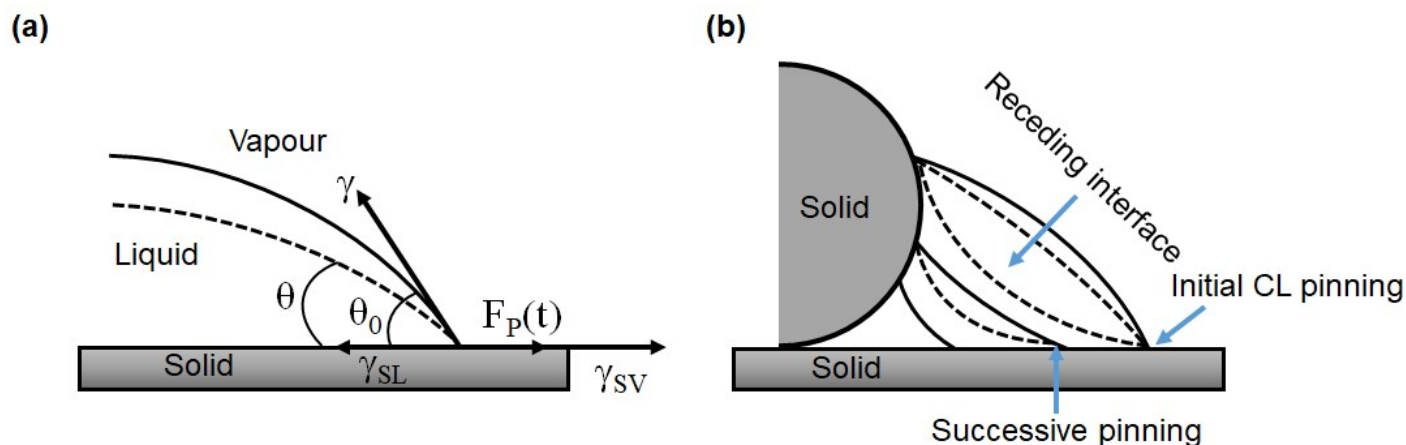


Fig. 5 Schematic representation of the drying drops. (a) Force balanced at the three phase contact line and (b) contact line dynamics of drying dispersion in the sphere-on-plate configuration.

Where $\theta(t)$ is the instantaneous contact angle and $F_P(t)$ is the instantaneous pinning force per unit length. A sessile drop deposited on the solid substrate evaporates in the CCR mode as schematically shown in Fig.5 (a). As the droplet continues to evaporate, $\theta(t)$ decreases and hence $F_P(t)$ increases. The pinning force, $F_P(t)$ takes a maximum possible value, F_{Pmax} when $\theta(t) = \theta_R$ which depends on drying conditions (such as temperature, humidity), the surface energies of the substrate and the fluid. At this instant, the contact line de-pins or slips and the evaporation occurs in constant contact angle (CCA) mode with $\theta(t) = \theta_R$ accompanied by a decrease in the contact diameter. In

the sessile drop configuration, the condition $\theta(t) < \theta_R$ limit is met at a later stage of the drying process ($t \geq 0.65t_f$).

When the drying of dispersion in the sphere-on-plate configuration is considered, a liquid bridge is formed between the flat plate and the spherical glass bead as shown in Fig.5 (b). Therefore, the drying of dispersion in this configuration involves two contact lines (flat substrate-water-air and spherical bead-water-air) instead of one three phase contact line in the sessile mode. At the early stages of drying ($t < 0.25t_f$), the contact line is pinned at both the surface of the spherical bead and the horizontal flat substrate as $\theta(t) > \theta_R$. The hydrophilic nature of the flat sub-

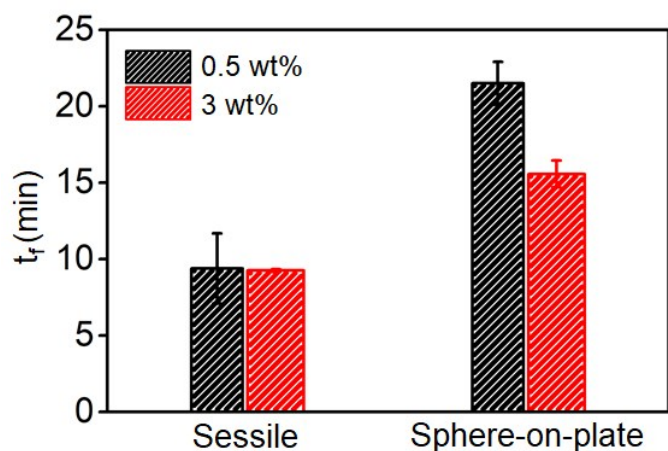


Fig. 6 A comparison of the lifetime, t_f , of the dispersions dried in the sessile and sphere-on-plate configuration.

strate and the spherical bead, as well as favorable droplet curvature helps in the pinning of the drying drop at this early stage as schematically shown in Fig.5 (b) [see also Fig. S4 in ESI†]. However, as the evaporation continues, the water-air interface recedes due to the continuous loss of water inducing a change in the interfacial curvature. This leads to decrease in the three phase contact angle at the two pinned contact lines and thus $\theta(t)$ approaches θ_R . Similar contact line dynamics has been reported for drying of a pure liquid in the sphere-on-plate configuration^{39,40}. The condition for the de-pinning of the contact line i.e., $\theta(t) < \theta_R$ is met at much earlier stage (approximately at $t \approx 0.25t_f$) in case of drying in the sphere-on-plate configuration. At this stage of drying, the contact line de-pins from the initial pinning point and jumps to a new pinning point as schematically shown in Fig.5 (b). At this point contact diameter and hence the interface curvature re-adjust until a quasi-equilibrium state is reached such that $\theta(t) > \theta_R$. In this way the contact line exhibits a “stick – slip” motion i.e. the contact line is pinned for a limited period when $\theta(t) > \theta_R$ and soon it de-pins when $\theta < \theta_R$ during the course of drying, which is also evident from the evolution of the normalized diameter vs evaporation time plots shown in Fig.4. This unusual stick-slip motion of the fluid schematically shown in Fig.5 (b), results in the formation of concentric-ring like deposit and is prominent at lower particle concentration ($\phi \approx 0.12$ -0.5%). However, at the later stage of drying ($t > 0.9t_f$), when the contact diameter is less than or equal to the diameter of the spherical bead, a continuous de-pinning is observed. This is confirmed from the continuous decrease in the contact diameter for $0.9t_f < t < t_f$.

The influence of drying configuration on the evaporation kinetics is further evident from the measurement of the total drying time (t_f), shown in Fig.6. The life time of the dispersion of same droplet volume that are dried in the sphere-on-plate configuration is significantly higher than that dried in the sessile mode. It is evident from Fig.4 (a) and (b) that the kinetics of drying irrespective of concentration of particles in the dispersion considered in this study is similar, however, significantly influenced by the drying configuration.

3.3 Concentric rings to concentric cracks and long-ranged assembly of particles

Drying aqueous drops containing hematite ellipsoids (pH=2) in sessile configuration always give coffee-ring deposit irrespective of the particle concentration as discussed, which is in agreement with earlier reports^{9,10}. An increase in the concentration of particles in the drying drop results in an increase in the thickness as well as width of the annular deposit. When the thickness of the particulate film exceeds a particular value, defined as the critical cracking thickness (CCT), the cracks appear in the particulate film^{41,42}. The particulate deposits adhered to the solid substrates are known to fail and give rise to cracks. These cracks are formed due to the release of the excess stress energy which is accumulated in the particulate film during the drying process^{29,33}. In the current study, the cracks in the annular region are prominent in the deposits obtained after the drying of dispersion containing particle at concentration, $\phi \geq 0.3$ wt% [See Fig. S5 in ESI†]. The microscopy images in Fig.7 shows that the particulate deposit resulting from drying the particle laden drop ($\phi \sim 4$ wt%) in the sessile drop configuration exhibit circular cracks which is limited to the annular ring region. This is due to the fact that most of the particles are deposited solely in this region [see Movie S1 in ESI†]. The micro-structure reveals that the ellipsoids in the ring region of the deposit are closed packed. The ellipsoids across the crack openings are aligned with their major axis parallel to the crack direction as shown by the encircled region in Fig.8. In general, the organisation of particles in the deposit is known to depend on the particle diffusion time scale, the hydrodynamic time scale, which is dictated by the fluid flow velocities⁴³ and presence of external field, if any. If the fluid velocity that brings the particles to the contact line is sufficiently low, the particles have enough time to arrange into a ordered assembly structure. The ellipsoids in the drying drop approach the contact line with their major axis parallel to the radial fluid motion. However, at the contact line, they experienced a hydrodynamic torque due to the radial outward flow of the solvent. The torque experienced by the ellipsoid results in the alignment of these particles with major axis parallel to the contact line. Thus, the alignment of particles in the deposit governs the direction of the crack propagation. The cracks follow the least resistance path giving rise to circular cracks⁴⁴. In Fig.8, the dashed encircled region shows the assembly of ellipsoids is across the thickness of the particulate film. Moreover, the ordered particle assembly is limited to the annular region and the arrangement of particles is disordered in the interior region of the deposits as shown in Fig.8.

Interestingly, the drying of drops containing hematite ellipsoids in the sphere-on-plate configuration shows “concentric – ring” to “concentric – crack” transition in the dried particulate deposit with an increase in the particle concentration. Optical microscopy images in Fig.7 clearly demonstrate that the dried particulate film resulting from drying of dispersion of ellipsoids at $\phi \geq 3$ wt% [see Fig. S6 in ESI†] in the sphere-on-plate configuration exhibit long-ranged concentric circular cracks [see Movie S2 in ESI†]. This is further confirmed from the intensity versus distance plot shown in Fig.7, which is an indirect measurement of the accumu-

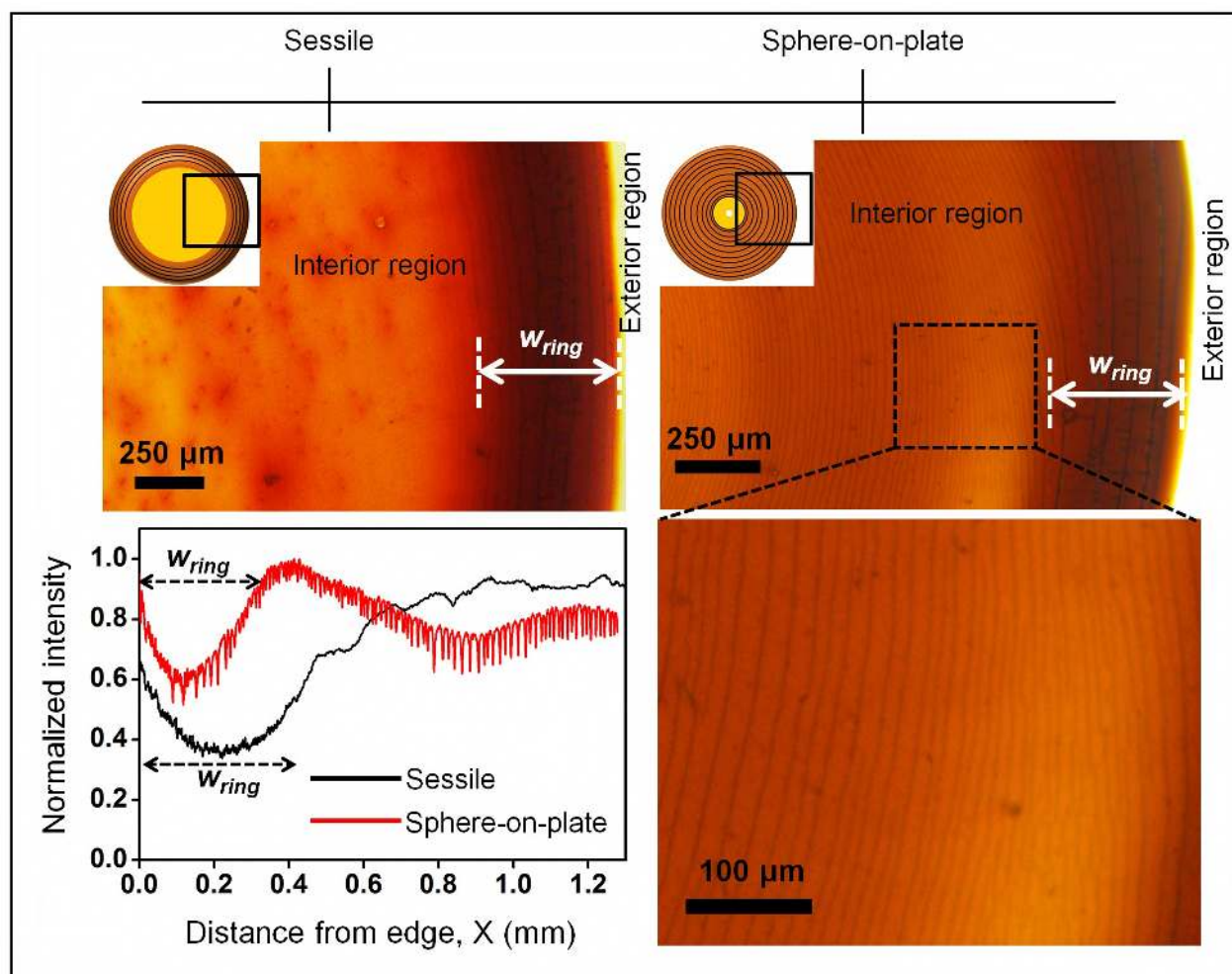


Fig. 7 The optical microscopy images of a part of the dried particulate film obtained upon drying of dispersions containing $\sim 4\text{wt}\%$ ellipsoids. The micrographs show that the region of the deposit over which the cracks form is strongly influenced by the drying configuration. The intensity profile confirms the formation of long-ranged circular cracks when the dispersions are dried in the sphere-on-plate configuration compared to the sessile drop drying. The dips in the intensity corresponds to the cracks in the particulate films.

lation of particles in the dried deposit. A lower intensity in the microscopy image corresponds to higher particle concentration and therefore, it is evident that the height of the deposit close to the contact line is higher for the case of drying in sessile configuration. It must also be noted from the intensity profile that the width of the annular deposit is higher for the sessile drop drying due to prolonged pinning compared to drying in sphere-on-plate configuration. However, the dried particulate deposit obtained in the sphere-on-plate configuration shows the accumulation of particle in the interior of the drop attributed due to the stick-slip motion of the contact line. Therefore, there is accumulation of enough particles throughout the deposit such that the thickness of the particulate film exceeds the critical cracking thickness (CCT), which is necessary for the nucleation of cracks and subsequent release of drying induced stresses. The dried particulate film are found to exhibit concentric cracks throughout the deposit i.e., over area as large as several square millimeters. The multiple dips, in the intensity plot for the drop dried in sphere-on-plate configuration shown in Fig.7 corresponds to the large number of concentric cracks in the dried particulate film. Note that each

dip corresponds to the cracks that appear black in the microscopy image. As mentioned earlier, the particles shows ordered assembly near the crack region with particles major axis parallel to the crack direction. The SEM micro-graphs shown in Fig.8 reveals a long ranged circular cracks and thus the long-ranged ordered assembly of ellipsoids in the particulate film is obtained in this drying configuration.

3.4 Effect of particle shape on the nature of crack and assembly of particle

In the previous section, we discussed that the particulate deposit obtained by drying of colloidal dispersion containing ellipsoids in the sphere-on-plate configuration shows a transition from concentric ring to long-ranged concentric cracks with an increase in the concentration of ellipsoids in the dispersion. In order to investigate the effect of particle shape, the drying experiments are performed under identical conditions, by considering aqueous dispersion of well characterized spherical colloids. The dispersion containing charge stabilized polystyrene (PS amidine latex)

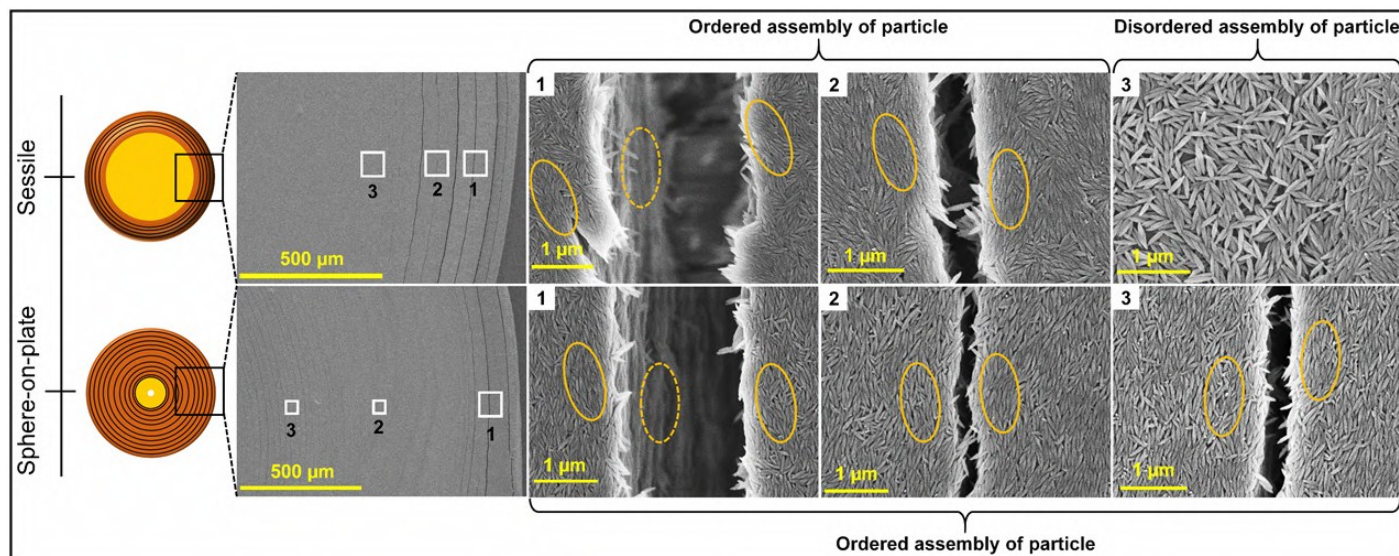


Fig. 8 The SEM micro-graphs show the assembly of particles near the vicinity of the crack. A clear dependence of the drying configuration on the assembly of particles in the dried particulate film is observed.

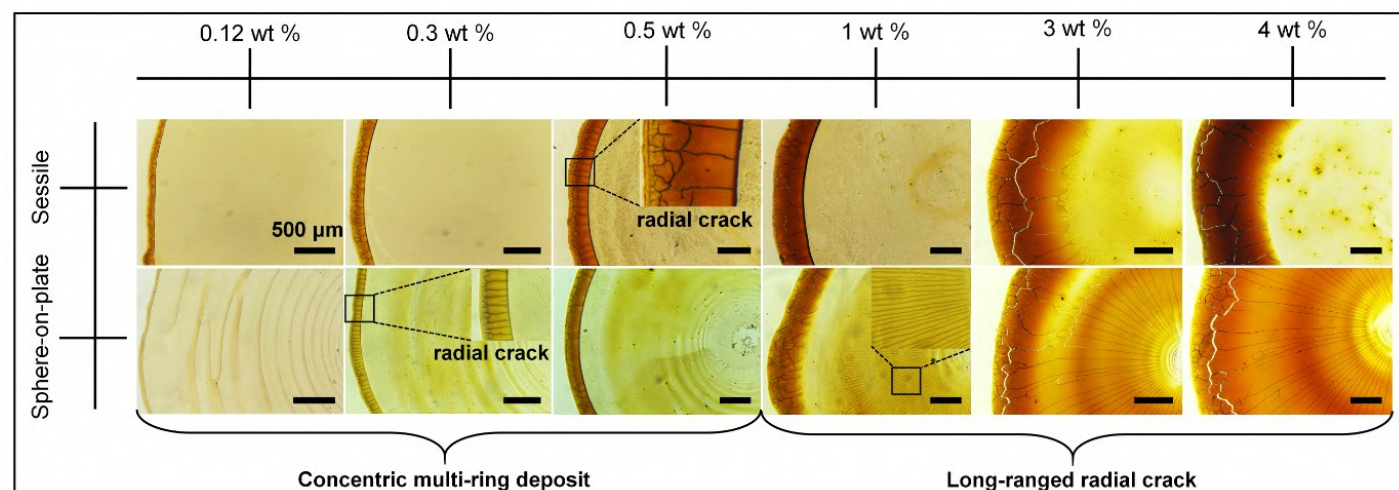


Fig. 9 The optical microscopy images of the part of the dried particulate deposit obtained by drying of drops containing spherical colloids. Deposits obtained by drying in sessile drop mode (top panel) show coffee-ring deposits and exhibit radial crack limited near the annular ring region. However, the deposits obtained by drying in the sphere-on-plate configuration (bottom panel) show concentric-ring to deposit with long-ranged radial crack with increase in concentration of particles in the dispersion. The scale bar in each image corresponds to 500 μm

spheres ($\alpha = 1$) of 200 nm diameter at various particles concentrations ($\phi \approx 0.12 - 4 \text{ wt}\%$) are dried in the two different drying configurations. Similar to the dispersion of ellipsoids, the final particulate deposit obtained by drying dispersion of spherical particles in the sessile drop mode always gives coffee-ring deposit i.e., deposition of particles at the three phase contact line irrespective of the particle concentration as shown in Fig.9. However, the height and width of the annular deposit strongly depends on the particles concentration. This is consistent with the similar observations in the particulate deposit obtained by drying of sessile drops containing hematite ellipsoids as shown in Fig.2 (a) and Fig.3 (a). In the particulate deposits of spherical colloids, the crack in the annular deposits are found to be oriented in the radial direction and the micro-structure of the deposit near the crack shows an

ordered assembly of particles as shown in Fig.10. The crack pattern and the particle assembly are similar to that reported in the past when the drops containing spherical particles are dried in the sessile configuration^{32,42,45,46}. At lower particle concentration ($\phi \approx 0.12 - 0.5 \text{ wt}\%$), the dispersion of spheres dried in the sphere-on-plate configuration show concentric-ring deposit as shown in Fig.9 which is similar to that observed for drying of aqueous dispersion containing ellipsoids. This is further confirmed from the height profile measurements shown in Fig. S2 in the ESI[†]. However, the microscopy images in Fig.9 reveal that the particulate deposit formed by the drying of dispersion containing spheres at higher particle concentrations ($\phi \geq 1 - 4 \text{ wt}\%$) in this drying mode show long-ranged radial cracks. To confirm that such deposits are independent of the nature of colloids used and solely depends on

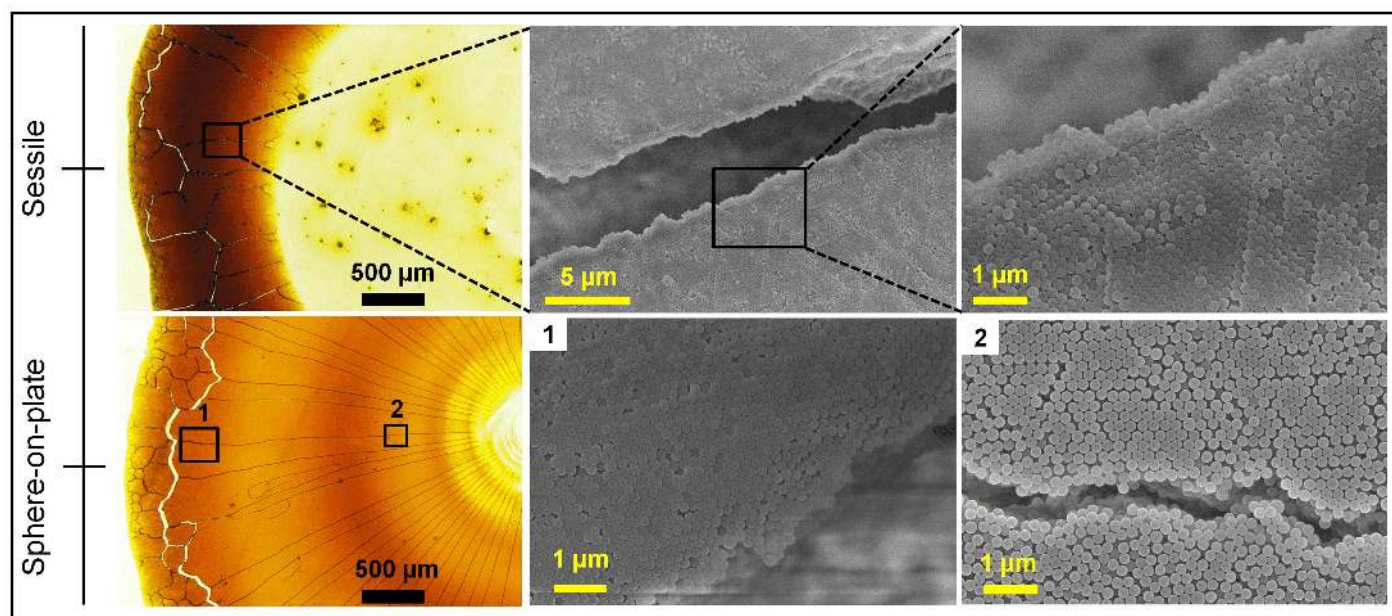


Fig. 10 The SEM micro-graphs shows the closed packed assembly of spherical particle in the vicinity of crack obtained by drying in sessile (top panel) and sphere-on-plate (bottom panel) configuration.

the particle shape as well as drying configuration, identical experiments are carried out using spherical colloidal silica (LUDOX-TMA) and the final deposit patterns as shown in the Fig. S7 in the ESI† are identical to the results reported for polystyrene particles. The SEM micro-graphs in Fig.10 depict the micro-structure near the crack. The deposit shows long range ordered assembly of the particle in the particulate films resulting from drying dispersion of *PS* spheres in the sphere-on-plate configuration i.e., from the edge of the deposit all the way to the center. Therefore, as evident from Fig.9 and Fig.10, the drying configuration as well as particle shape contribute to the nature of the deposit, crack morphology and the micro-structure of the particles in the vicinity of the cracks.

4 Conclusions

In summary, the influence of the drying configuration, particle shape and particle concentration on the nature of the deposit patterns left after the drying of colloidal dispersion are experimentally investigated. While drying of dispersion in the sessile drop mode produce coffee-ring deposit, irrespective of the particle concentrations ($\phi \sim 0.12\text{--}4.0\text{ wt}\%$), the drying of dispersion at particle concentration $\phi \sim 0.12\text{--}0.5\text{ wt}\%$ in the sphere-on-plate configuration results in deposits with multiple concentric-rings. The differences in the dried deposit patterns is explained based on the differences in the contact line dynamics in the two drying configurations. While the dispersion evaporated in the sessile mode show constant contact radius (*CCR*) mode for majority of the drying period, whereas in the sphere-on-plate configuration, a stick-slip motion of the contact line is observed. At higher particle concentrations, $\phi \geq 1\text{ wt}\%$, the dispersion dried in sphere-on-plate configuration reveal a change in the micro-structure of the deposit from “concentric – rings” to “concentric – cracks”. These cracks in the particulate film arise due to the release of the excess

capillary stress energy, accumulated during the course of drying. Interestingly, the formation of concentric cracks is limited to annular region of the coffee-ring patterns in the sessile drop drying. However, in the sphere-on-plate mode, the concentric cracks are long-ranged and appear throughout the particulate film i.e., from the edge all the way to the center. Finally, the nature of crack in the particulate film are observed to depend on the shape of the constituent particle in the dispersion that is dried. We found that the dispersion of ellipsoids dried in the sphere-on-plate configuration show long-ranged circular cracks and the cracks morphology changes to radial when the shape of the constituent particles in the dispersion is spherical. The present study provides a promising approach to fabricate the hierarchical ordered structured materials which have potential application in electronics, lithography and in materials engineering.

Acknowledgment

We would like to acknowledge the Goniometer facility at the soft materials lab (Prof. Dilip K Satapathy, Department of Physics, IIT Madras). We acknowledge MEMS Lab (Department of Electrical Engineering, IIT Madras) for the optical surface profilometry and the scanning electron microscopy (SEM) facility in the Department of Chemical Engineering, IIT Madras (procured through DST-FIST grant).

Notes and references

- 1 W. Han and Z. Lin, *Angewandte Chemie International Edition*, 2012, **51**, 1534–1546.
- 2 J. R. Trantum, D. W. Wright and F. R. Haselton, *Langmuir*, 2011, **28**, 2187–2193.
- 3 T.-S. Wong, T.-H. Chen, X. Shen and C.-M. Ho, *Analytical chemistry*, 2011, **83**, 1871–1873.

- 4 R. D. Deegan, O. Bakajin, T. F. Dupont, G. Huber, S. R. Nagel and T. A. Witten, *Nature*, 1997, **389**, 827.
- 5 R. D. Deegan, O. Bakajin, T. F. Dupont, G. Huber, S. R. Nagel and T. A. Witten, *Physical review E*, 2000, **62**, 756.
- 6 H. Hu and R. G. Larson, *The Journal of Physical Chemistry B*, 2006, **110**, 7090–7094.
- 7 P. J. Yunker, D. J. Durian and A. G. Yodh, *Physics Today*, 2013, **66**, 60.
- 8 P. J. Yunker, T. Still, M. A. Lohr and A. Yodh, *Nature*, 2011, **476**, 308.
- 9 V. R. Dugyala and M. G. Basavaraj, *Langmuir*, 2014, **30**, 8680–8686.
- 10 R. Mondal, S. Semwal, P. L. Kumar, S. P. Thampi and M. G. Basavaraj, *Langmuir*, 2018, **34**, 11473–11483.
- 11 R. Bhardwaj, X. Fang, P. Somasundaran and D. Attinger, *Langmuir*, 2010, **26**, 7833–7842.
- 12 V. R. Dugyala and M. G. Basavaraj, *The Journal of Physical Chemistry B*, 2015, **119**, 3860–3867.
- 13 I. Sandu, M. Dumitru, C. T. Fleaca and F. Dumitrache, *Photonics and Nanostructures-Fundamentals and Applications*, 2018, **29**, 42–48.
- 14 S. Xu and E. Kumacheva, *Journal of the American Chemical Society*, 2002, **124**, 1142–1143.
- 15 Z. Mitov and E. Kumacheva, *Physical Review Letters*, 1998, **81**, 3427.
- 16 V. X. Nguyen and K. J. Stebe, *Physical Review Letters*, 2002, **88**, 164501.
- 17 S. Tarafdar, Y. Y. Tarasevich, M. Dutta Choudhury, T. Dutta and D. Zang, *Advances in Condensed Matter Physics*, 2018, **2018**, year.
- 18 D. Mampallil, *Resonance*, 2014, **19**, 123–134.
- 19 R. Bhardwaj, *Colloid and Interface Science Communications*, 2018, **24**, 49–53.
- 20 J. Leng, *Physical Review E*, 2010, **82**, 021405.
- 21 Z. Lin and S. Granick, *Journal of the American Chemical Society*, 2005, **127**, 2816–2817.
- 22 J. Xu, J. Xia and Z. Lin, *Angewandte Chemie International Edition*, 2007, **46**, 1860–1863.
- 23 M. Liu, Z. Huo, T. Liu, Y. Shen, R. He and C. Zhou, *Langmuir*, 2017, **33**, 3088–3098.
- 24 K. Mae, H. Toyama, E. Nawa-Okita, D. Yamamoto, Y.-J. Chen, K. Yoshikawa, F. Toshimitsu, N. Nakashima, K. Matsuda and A. Shioi, *Scientific reports*, 2017, **7**, 5267.
- 25 K. Joshi and J. F. Gilchrist, *Journal of colloid and interface science*, 2017, **496**, 222–227.
- 26 V. R. Dugyala and M. G. Basavaraj, *RSC Advances*, 2015, **5**, 60079–60084.
- 27 L. Goehring, R. Conroy, A. Akhter, W. J. Clegg and A. F. Routh, *Soft Matter*, 2010, **6**, 3562–3567.
- 28 F. Giorgiutti-Dauphiné and L. Pauchard, *Journal of Applied Physics*, 2016, **120**, 065107.
- 29 L. Goehring, A. Nakahara, T. Dutta, S. Tarafdar and S. Kit-sunezaki, *Desiccation cracks and their patterns: Formation and Modelling in Science and Nature*, John Wiley & Sons, 2015.
- 30 W. P. Lee and A. F. Routh, *Langmuir*, 2004, **20**, 9885–9888.
- 31 H. Lama, M. G. Basavaraj and D. K. Satapathy, *Physical Review Materials*, 2018, **2**, 085602.
- 32 H. Lama, M. G. Basavaraj and D. K. Satapathy, *Soft matter*, 2017, **13**, 5445–5452.
- 33 H. Lama, R. Mondal, M. G. Basavaraj and D. K. Satapathy, *Journal of colloid and interface science*, 2018, **510**, 172–180.
- 34 M. Ocaña, M. Morales and C. Serna, *Journal of colloid and interface science*, 1999, **212**, 317–323.
- 35 H. Y. Erbil, *Advances in colloid and interface science*, 2012, **170**, 67–86.
- 36 M. E. Shanahan, *Langmuir*, 1995, **11**, 1041–1043.
- 37 P.-G. De Gennes, F. Brochard-Wyart and D. Quéré, *Capillarity and Wetting Phenomena*, Springer, 2004, pp. 33–67.
- 38 J. M. Stauber, S. K. Wilson, B. R. Duffy and K. Sefiane, *Physics of fluids*, 2015, **27**, 122101.
- 39 M. J. Neeson, R. R. Dagastine, D. Y. Chan and R. F. Tabor, *Soft Matter*, 2014, **10**, 8489–8499.
- 40 F. Orr, L. Scriven and A. P. Rivas, *Journal of Fluid Mechanics*, 1975, **67**, 723–742.
- 41 V. Lazarus and L. Pauchard, *Soft Matter*, 2011, **7**, 2552–2559.
- 42 M. S. Tirumkudulu and W. B. Russel, *Langmuir*, 2005, **21**, 4938–4948.
- 43 Á. G. Marín, H. Gelderblom, D. Lohse and J. H. Snoeijer, *Physical review letters*, 2011, **107**, 085502.
- 44 V. R. Dugyala, H. Lama, D. K. Satapathy and M. G. Basavaraj, *Scientific reports*, 2016, **6**, 30708.
- 45 F. Giorgiutti-Dauphiné and L. Pauchard, *The European Physical Journal E*, 2014, **37**, 39.
- 46 L. Pauchard, F. Parisse and C. Allain, *Physical Review E*, 1999, **59**, 3737.